Electron tunneling dynamics between two-dimensional and zero-dimensional quantum systems: Contributions of momentum matching, higher subbands, and phonon-assisted processes

A. R. Korsch,* C. Ebler, G. N. Nguyen, S. Scholz, A. D. Wieck, and A. Ludwig
Lehrstuhl für Angewandte Festkörperphysik, Ruhr-Universität Bochum, Universitätsstraße 150, D-44780 Bochum, Germany

(Received 2 May 2020; revised 11 June 2020; accepted 15 June 2020; published 9 July 2020)

We investigate tunneling dynamics of electrons from an ensemble of self-assembled InAs quantum dots into the subbands of a two-dimensional electron gas (2DEG). LO-phonon-assisted tunneling processes and tunneling into higher subbands of the 2DEG electronic structure cause distinct resonances in the evolution of the tunneling rate as a function of the energy detuning between quantum dot and 2DEG ground state. By devising a semiquantitative model, we identify the momentum mismatch between the quantum dot and 2DEG wave function as the crucial quantity governing the evolution of the tunneling rate. In particular, we demonstrate that this mechanism along with the availability of tunneling into the second 2DEG subband allows for tuning of the tunneling rate by more than two orders of magnitude.

DOI: 10.1103/PhysRevB.102.035413

I. INTRODUCTION

Self-assembled InAs quantum dots (QDs) are a prototypical zero-dimensional solid-state quantum system due to their three-dimensional confinement of charge carriers. The resulting discrete energy level structure combined with high integratability in the mature GaAs material platform makes them a promising system for applications in future quantum information [1] and memory devices [2]. Tunnel coupling of the QD energy levels to a reservoir of charge carriers is essential for recent electronic [3,4] as well as optical experiments [5–7] on QDs, as it allows for controlling the QD charge state [8]. The tunneling rate is governed by the transmission probability of charge carriers through the potential barrier [9], as well as the lateral wave function overlap between the two quantum systems in the plane perpendicular to the direction of tunneling [10,11] (also referred to as momentum matching).

The physics of tunneling into and out of QDs was studied extensively in resonant tunneling diode structures, in which QDs are embedded into a potential barrier between two charge carrier reservoirs. These devices enabled the observation of a multitude of tunneling phenomena such as Fermi-edge singularities [12] as well as spectroscopy of properties of occupied states in the charge carrier reservoirs such as Landau level splitting in a two-dimensional electron gas (2DEG) [13,14]. The lateral wave function overlap of the quantum systems has been thoroughly investigated in magnetotunneling spectroscopy. In these experiments, an in-plane magnetic field allows for controlled displacement of the emitter wave function in a charge carrier reservoir with respect to the QD wave function in momentum space. This mechanism was harnessed to image the momentum space distribution of the wave function [15,16].

In contrast to resonant tunneling diodes, the recently invented method of transconductance spectroscopy uses the current through a 2DEG as a sensor for electron tunneling processes into and out of QDs [17–19]: tunneling processes lead to a change in conductance of the two-dimensional electron channel over time from which the electron tunneling rate can be determined directly. This distinguishes transconductance spectroscopy from experiments on resonant tunneling diode structures, in which only the tunneling current through the QD energy levels between two charge carrier reservoirs is accessible. In particular, in transconductance spectroscopy tunneling dynamics into and out of the QDs are accessible independently, leading to observations of several new phenomena: the asymmetry of in- and out-tunneling rates due to degeneracy of the involved states [20], an all-electrical measurement of the singlet-triplet spin relaxation time [21], and investigations of momentum matching between QDs and unoccupied states in the first electronic subband in the 2DEG [11].

Here, we use all-electrical transconductance spectroscopy to investigate tunneling processes of electrons from singly charged QDs into the subbands of a 2DEG. As a function of increasing energy detuning of the charged QD states above the 2DEG Fermi energy we find prominent increases in the tunneling rate when additional tunneling processes become energetically available: the presence of higher subbands in the 2DEG and phonon-assisted tunneling leads to an all-electrical tuning of the tunneling rate over more than two orders of magnitude. We find that lateral momentum matching between the QD and 2DEG wave functions crucially governs the evolution of the tunneling rate.

II. MATERIALS AND METHODS

The sample structure consists of InAs QDs embedded in an inverted high electron mobility transistor structure grown

*alexander.korsch@alumni.rub.de

 ©2020 American Physical Society

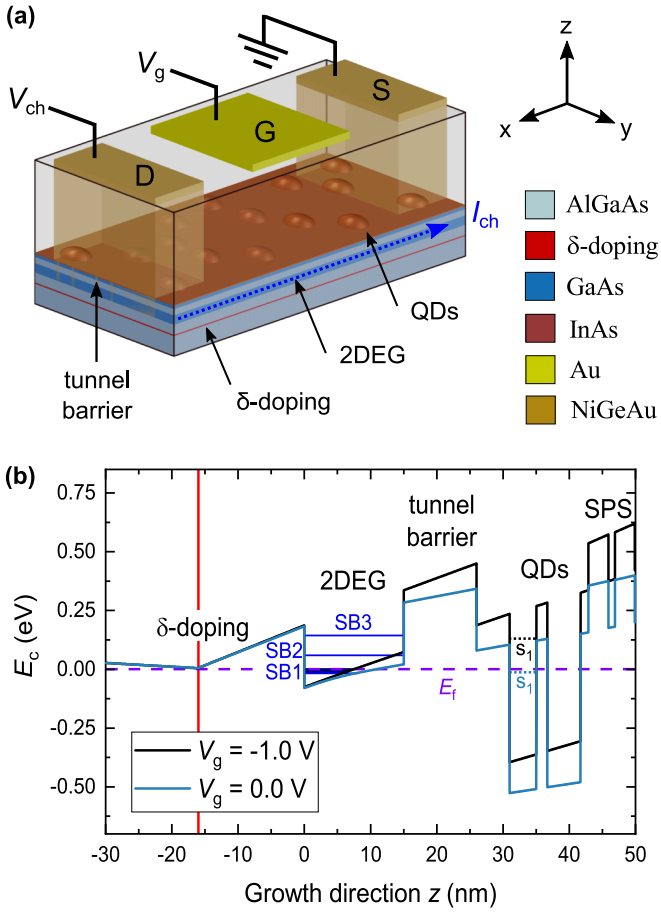

FIG. 1. (a) Schematic sample structure of the device. Channel voltage V_{ch} between source (S) and drain (D) contacts drives a current I_{ch} in the 2DEG channel. Gate voltage V_g controls the conductance of the 2DEG channel below the gate and shifts the QD energy levels. (b) Conduction band structure in the 2DEG-QD region along the z direction and subband (SB) energy levels calculated using nextnano simulations (at $V_g = 0.0$ V). Quantum dots are represented as InAs quantum wells and the electronic QD ground state s_1 of the first QD layer is indicated schematically. Thin AlAs layers on top of the QDs are not shown.

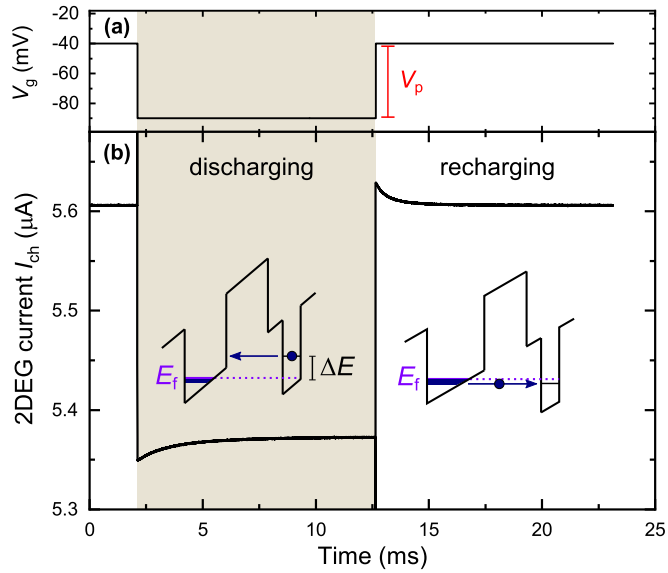

FIG. 2. (a) Exemplary sequence of gate voltage pulses for pulse voltage $V_p = -50$ mV; (b) resulting 2DEG current response as a function of time. Insets in (b) show discharging of the initially singly charged QDs via electron tunneling into the 2DEG when a negative gate voltage pulse is applied (left) and subsequent recharging (right). Overshoots of the current at the start and end of the voltage pulse are related to capacitive charging processes in the transistor channel.

by molecular beam epitaxy on a (100)-oriented GaAs substrate (cf. Fig. 1). Self-assembled QDs with lateral diameters of approximately 25 nm and height of approximately 4 nm are grown at 525 °C under established growth conditions in the Stranski-Krastanov growth mode [22] using the indium-flush technique [23]. The QDs are separated by a 5 nm GaAs and 11 nm $Al_{0.3}Ga_{0.7}As$ tunnel barrier from a 15 nm quantum well. A silicon δ-doped layer separated from the quantum well by a 16 nm $Al_{0.3}Ga_{0.7}As$ spacer populates the quantum well with electrons, leading to the formation of a 2DEG. The device contains a second layer of QDs, which is not used in this study and does not influence the electronic properties of the first QD layer in the investigated charge tuning range (see Supplemental Material [24]). Upon each QD layer, a thin 0.3 nm AlAs layer is grown, which can be used to suppress electronic wetting layer states [25], but is not of relevance for this work. The first (second) QD layer is capped with a 5.4 nm (5.9 nm) GaAs layer. A short-periodic superlattice (SPS) consisting of 35 periods of alternating 3 nm AlAs and 1 nm GaAs layers blocks the current between the 2DEG and metal gate. The SPS is capped with another 5 nm GaAs layer. From the grown wafer, 5×5 mm^2 pieces are cleaved and a field effect transistor structure consisting of annealed NiGeAu source and drain electrodes and a gold gate are deposited. Figure 1 shows the finalized device and conduction band structure along the growth direction in the QD-2DEG region. Note that in Fig. 1(b) the thin AlAs layers on top of the QDs are not shown for simplicity as their exact position shifts during the growth process [25]. Measurements are conducted in a liquid helium bath cryostat at a temperature of 4.2 K.

The gate voltage V_g modulates the current through the 2DEG channel by changing the charge carrier density and thus the conductance. At the same time, the QD energy levels are shifted to lower (higher) energies by a positive (negative) gate voltage. If the energy levels are tuned below the Fermi energy in the 2DEG, electrons can tunnel from the 2DEG into unoccupied QD energy levels. The change in conductance is measured as a change in the current across the two-dimensional electron channel I_{ch}.

In our transconductance spectroscopy experiment, we charge approximately half of the QDs in the ensemble at a fixed dc voltage $V_{dc} = -40$ mV with one electron (see Supplemental Material for full QD charging spectrum). By applying a negative voltage pulse V_p to the transistor gate [see Fig. 2(a)], the charged QD energy levels are shifted above the Fermi energy E_f by an energy detuning ΔE, inducing electron tunneling into free 2DEG states as shown in the insets of Fig. 2(b). A more negative pulse voltage leads to an increasing detuning of the charged QD states above the

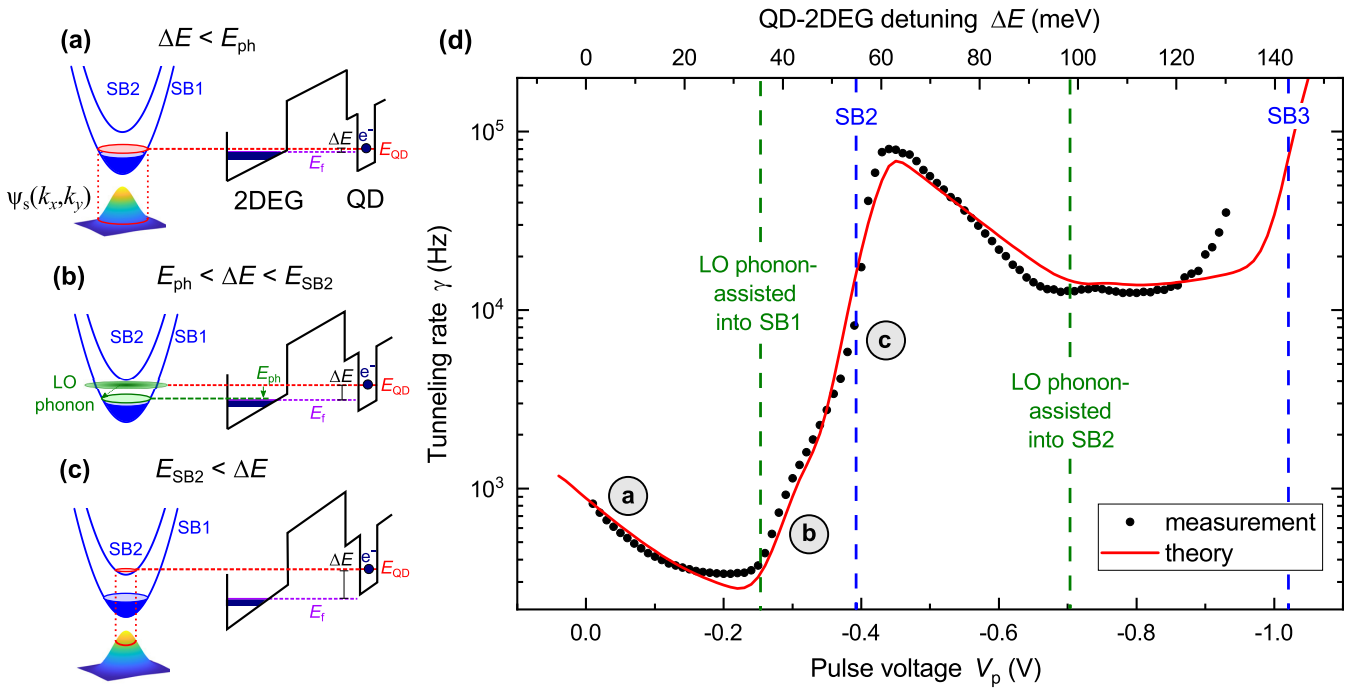

FIG. 3. (a)–(c) Schematic illustration of tunneling mechanisms. (a) Elastic tunneling into the first 2DEG subband: the size of the Fermi circle (red) within one subband increases and thus its momentum space overlap with the lateral s-state QD wave function $\psi_s(k_x, k_y)$ decreases towards higher energy detuning. (b) Inelastic tunneling assisted by emission of a LO phonon into the first subband; (c) elastic tunneling into the second 2DEG subband. Schematic illustrations of LO phonon-assisted tunneling into the second and elastic tunneling into the third subband are not shown for simplicity as they are conceptually identical to processes shown in (b) and (c), respectively. (d) Electron tunneling rate γ as a function of applied pulse voltage V_p (bottom axis) and QD-2DEG detuning ΔE (top axis). At higher ΔE, tunneling into the second and eventually the third subband as well as tunneling assisted by emission of LO phonons becomes energetically possible (indicated by vertical dashed lines). Black circles are experimental data and the solid red line is the result of a semiquantitative model [cf. Eq. (1) in Sec. IV]. Three large gray circles labeled a, b, c indicate the tunneling mechanisms in the respective regions, which are illustrated schematically in panels (a), (b), and (c).

Fermi energy, allowing for the investigation of discharging processes in a highly nonequilibrium electron configuration [4,11]. The discharging processes of electrons tunneling from the QDs into the 2DEG lead to an increase of the channel current over time [see Fig. 2(b)] as the electron charge density in the 2DEG increases. An exponential fit to the discharging transient yields the electron tunneling rate [17]. After each discharging pulse, the QDs are recharged with one electron by returning to the initial dc voltage $V_{dc} = -40$ mV. To enhance the signal to noise ratio of the measurement, we repeat the same measurement N times and average the time traces of the channel current ($N = 11000$ for $|V_p| \leqslant 0.45$ V; $N = 22000$ for $|V_p| \geqslant 0.46$ V).

For a quantitative analysis, the value of the detuning ΔE of the charged QD energy levels above the Fermi energy has to be known. The energy shift at the QD position induced by a change in applied gate voltage V_p follows a linear lever arm law $\Delta E = -eV_p/\lambda$ with elementary charge e and leverarm factor λ [8]. We determine the leverarm factor $\lambda = 7.15$ from 1D Poisson-Schrödinger simulations of the heterostructure using the software NEXTNANO by calculating the position of the band edge at the QD position as a function of gate voltage [26]. Note that the QDs are included in the NEXTNANO simulations only as quantum wells without three-dimensional structure as we are only interested in the voltage-induced change of the band edge at the QD position. The tilt of the band structure due to a voltage applied to the gate also shifts the energy levels of electronic subbands in the 2DEG. From the band structure simulations, we extract the shift of the first three subband edges E_{SB1}, E_{SB2}, and E_{SB3} at all gate voltages.

III. RESULTS

Figure 3(d) shows the tunneling rate as a function of applied negative pulse voltage (bottom axis) or QD-2DEG energy detuning ΔE (top axis). As a function of detuning, the tunneling rate shows a complex, highly nonmonotonous evolution. While for the smallest detunings ΔE, electrons tunnel elastically from the QDs into the first 2DEG subband, additional tunneling mechanisms become energetically available with increasing energy detuning as follows.

(i) LO phonon-assisted tunneling into the first subband ($\Delta E \geqslant E_{ph}$, where E_{ph} is the LO phonon energy).

(ii) Elastic tunneling into the second subband ($\Delta E \geqslant E_{SB2}$).

(iii) LO phonon-assisted tunneling into the second subband ($\Delta E \geqslant E_{SB2} + E_{ph}$).

(iv) Elastic tunneling into the third subband ($\Delta E \geqslant E_{SB3}$).

Dashed lines in Fig. 3(d) indicate the values of the energy detuning ΔE at which the respective tunneling mechanisms first become available. These values are calculated from NEXTNANO simulations as the crossover of the QD energy

level with the required energy for each tunneling mechanism. All features observed in the measurement are broadened due to QD ensemble inhomogeneity (spectral FWHM $\delta E_{\mathrm{inh}} = 13$ meV; see Supplemental Material). In the following subsections, we discuss how the availability of different tunneling channels leads to the evolution of the tunneling rate in Fig. 3(d).

A. Elastic tunneling into the first subband

At low detuning $\Delta E < 35$ meV, electron tunneling occurs elastically into the first subband of the 2DEG electronic structure. In this regime, the tunneling rate in Fig. 3(d) decreases with increasing detuning. This observation is contrary to the increasing transmission of the tunneling barrier due to a reduced effective barrier height and tunneling length at higher ΔE. In a similar experiment, Zhou *et al.* showed that this behavior is caused by the decreasing overlap of the QD and 2DEG wave functions in momentum space [11]: electronic states in the 2DEG are plane waves. For elastic tunneling into the first 2DEG subband, free final states in the 2DEG are located on a circle with radius $k_{\mathrm{F,SB1}} = [2m_{\mathrm{e}}^{*}(\Delta E + E_{\mathrm{f}})/\hbar^{2}]^{1/2}$ on the paraboloid lateral dispersion of the 2DEG in the effective-mass (m_{e}^{*}) approximation—the Fermi circle. With increasing energy detuning ΔE, the radius of the Fermi circle increases. In the common parabolic approximation of the lateral QD confinement potential [27], the in-plane wave function of the ground s state in the QDs is given by a two-dimensional Gaussian wave function, both in real and momentum space. Consequently, the overlap of the Fermi circle with the initial electronic state in the QDs decreases as the radius of the Fermi circle increases. This tunnel mechanism is illustrated schematically in Fig. 3(a).

At higher detuning $35\ \mathrm{meV} < \Delta E < 62$ meV, the tunneling rate rapidly increases by more than two orders of magnitude. This increase occurs in two steps, one starting at $\Delta E = 35$ meV and the second around $\Delta E = 50 \pm 1$ meV. We assign these phenomena to the availability of additional tunneling channels if the charged QD energy state is detuned to highly nonequilibrium electronic configurations. Note that these features were not observed in the work by Zhou *et al.* [11] because they only investigated the regime of small detunings ΔE. We discuss the origins of these features in the following two subsections III B and III C.

B. LO phonon-assisted tunneling into the first subband

The energy of the first increase corresponds closely to typical energies of optical phonons in GaAs $E_{\mathrm{ph}} = 35.9$ meV [28]. At energy detunings equal to or higher than the optical phonon energy, inelastic tunneling processes with emission of an optical phonon into final states at a reduced energy $\Delta E - E_{\mathrm{ph}}$ in the 2DEG can occur in parallel to the elastic tunneling channel. An optical phonon replica of the electronic ground state in GaAs-based QD devices has been demonstrated before in transconductance spectroscopy experiments [18] and LO phonon-assisted tunneling has been shown to be an efficient mechanism for electron tunneling in coupled QD-2DEG structures [28].

Phonon-assisted tunneling couples initial states in the QDs and final states in the 2DEG indirectly in momentum space due to the finite phonon momentum [see Fig. 3(b)]. As a consequence, at any energy detuning ΔE, tunneling of an electron from any point in momentum space of the QD wave function into any free state on the 2DEG electron dispersion at energy $\Delta E - E_{\mathrm{ph}}$ is possible by emission of a phonon with appropriate momentum. As the density of final states in each subband of the 2DEG is constant, the phonon-assisted tunneling rate does not dependent strongly on the energy detuning for a single QD. Nevertheless, this process leads to a continuous increase of the observed tunneling rate in Fig. 3(d) around $\Delta E \geqslant E_{\mathrm{ph}}$ due to the spectral broadening of the QD ensemble: as the energy detuning ΔE increases further above the phonon energy E_{ph}, more QDs have access to the phonon-assisted tunneling channel increasing the overall tunneling rate.

C. Elastic tunneling into the second subband

The second, very abrupt increase of the tunneling rate, starting around $\Delta E = 50 \pm 1$ meV, can be attributed to tunneling of electrons from the QDs into the second subband of the 2DEG. NEXTNANO simulations of the heterostructure show that the QD charge state crosses the energetic position of the second subband for an applied pulse voltage of $V_{\mathrm{p}} = -0.39$ V, corresponding to an energy detuning of $\Delta E = 55$ meV. Considering the influence of inhomogeneous ensemble broadening of the quantum dots in the measurement, this value is in good agreement with the experimentally observed energy detuning $\Delta E = 50 \pm 1$ meV at which the second, abrupt increase of the tunneling rate begins.

At cryogenic temperature of 4.2 K, almost all electronic states in the second subband are unoccupied. If the negative voltage pulse shifts the charged electron state in the QDs into resonance with the bottom edge of the second subband, electrons find free final states in the 2DEG at $k_{\mathrm{F,SB2}} = 0$. Hence the radius of the Fermi circle is minimal and the resulting momentum space overlap with the Gaussian initial state in the QDs is maximized resulting in highly efficient electron tunneling. Figure 3(c) illustrates this mechanism. Due to the large overlap of the wave functions in momentum space and since the electronic density of states in the 2DEG is constant in each subband, the tunneling rate increases abruptly once free final states in the second subband become available. In the range of energy detunings between 62 and 95 meV, the tunneling rate decreases again, owing to the increasing size of the Fermi circle—both in the first and second 2DEG subband.

D. LO phonon-assisted tunneling into the second subband

Between energy detunings of 95 to 110 meV, the tunneling rate remains nearly constant with a slight peak at $\Delta E = 105$ meV. From NEXTNANO band structure simulations, we calculate the crossover of the charged QD state with phonon-assisted tunneling processes into the second subband of the 2DEG to occur at an energetic detuning of $\Delta E = 98$ meV. This value agrees approximately with the position of the small peak in the tunneling rate. At such high detunings, emission of an optical phonon allows electron tunneling again into final

states at $k_{F,SB2} = 0$. The additional tunneling channel again increases the total tunneling rate.

E. Elastic tunneling into the third subband

Lastly, for detunings higher than $\Delta E = 110$ meV, the tunneling rate increases. Above $\Delta E = 130$ meV, where the channel conductance is already rather low due to the highly negative pulse voltage, no tunneling transients can be detected anymore because the time constants of the processes become too short for the time resolution of our experiment. The observed increase of the tunneling rate in this range may be related to the presence of a third subband in the 2DEG. At resonance with the bottom edge of the third subband, tunneling can again occur at $k_{F,SB3} = 0$. Additionally, the highly negative applied gate voltage tilts the bands so that the effective tunneling barrier height and length are significantly reduced compared to tunneling processes on resonance with the second subband starting around $\Delta E = 50$ meV. Therefore, the barrier transmission is increased and tunneling occurs at an even higher rate. The crossover of the QD state with the bottom edge of the third subband state is theoretically predicted from NEXTNANO simulations to occur at $\Delta E = 143$ meV. This value is significantly higher than the observed resonance in the experimental data. However, the third subband energy level is located at a high energy within the quantum well only 45 meV below the band edge of the AlGaAs barrier, separating the quantum well from the region of δ doping [see Fig. 1(b)]. Hence the third subband wave function can strongly hybridize with weakly confined states in deeper layers, decreasing the energy of the hybridized state and thus qualitatively explaining the deviation.

Lastly, we note that in Fig. 3(d) we do not observe signatures of a Fermi-edge singularity, i.e., a distinct power-law evolution of the tunneling rate when the QD level is close to resonance with the 2DEG Fermi energy due to many-body interactions of the tunneling electron with the Fermi sea in the 2DEG. Fermi-edge singularities were observed in resonant tunneling diode structures [12,29]. In our experiment, however, such a resonance is smeared out strongly due to temperature (4.2 K in our experiment in contrast to, for example, 40 mK in Ref. [12]) and the presence of the QD ensemble broadening inhibiting the observation. The absence of this feature is consistent with previous transconductance spectroscopy studies on similar samples under the same conditions [11].

IV. MODELING OF THE TUNNELING RATE

To underpin our proposed assignment of the observed features, we develop a semiquantitative model of the tunneling rate as a function of QD-2DEG detuning ΔE, solely based on the tunneling barrier transmission T and the lateral wave function overlap of 2DEG and QD states. The tunneling rate $\Gamma(\Delta E)$ is given by the sum of all energetically available tunneling channels:

$$\Gamma(\Delta E) = \nu T \left(\sum_{l=1}^{3} S_l(\Delta E) + \sum_{m=1}^{2} P_m(\Delta E) \right), \qquad (1)$$

where S_l are the respective overlap integrals of initial and final states for elastic tunneling processes into the three 2DEG subbands, ν is an unknown attempt frequency, and P_m are the contributions of phonon-assisted tunneling processes discussed below. The overlap integrals are given by

$$S_l(\Delta E) = |\langle \Phi_{\mathbf{k}_F,l} | \Psi_{QD} \rangle|^2 \Theta(\Delta E - E_l), \qquad (2)$$

where E_l are the bottom edge energy levels of the respective 2DEG subbands and Θ is the Heaviside step function. The subband edges and their shifts as a function of the applied negative pulse voltage are obtained from NEXTNANO simulations as described in Sec. II. We assume plane waves $\Phi_{\mathbf{k}_F}$ as 2DEG states with wave vectors on the Fermi circle with radius $k_{F,l} = [2m(\Delta E - E_l)/\hbar^2]^{1/2}$. The lateral QD wave function in the well-established approximation of a parabolic confinement potential in the x-y plane is given by

$$\Psi_{QD} = 1/(\sqrt{\pi} l_{conf}) \exp\left[-(x^2 + y^2)/\left(2l_{conf}^2\right)\right], \qquad (3)$$

assuming rotationally symmetric QDs with characteristic electron confinement length l_{conf} [27].

In accordance with our discussion of the phonon-assisted tunneling mechanism in Sec. III B, we assume an approximately constant tunneling rate for the phonon-assisted tunneling channels, which become available once the energy detuning crosses the required energy:

$$P_m(\Delta E) = \alpha_m \Theta(\Delta E - E_m - E_{ph}), \qquad (4)$$

where $E_{ph} = 35.9$ meV is the energy of LO phonons in GaAs [28], E_m is the bottom edge energy level of the 2DEG subband, and α_m is a fitting parameter for the phonon-assisted tunneling rate.

The change in barrier transmission T is calculated using a Wentzel-Kramers-Brillouin approximation. Calculations are performed for a single QD and broadening is introduced by convoluting the numerical result of (1) with the product of a Gaussian (FWHM $= \delta E_{inh} = 13$ meV, corresponding to the spectral width of the QD ensemble) and a Fermi distribution at temperature T_f. The latter takes into account that only half of the s_1 states in the QD ensemble are charged in our experiment and that charging occurs by tunneling from the broadened Fermi edge in the 2DEG. The absolute rate value is adjusted to the first data point in Fig. 3(d) at $V_p = -0.01$ V to allow for comparison with the data and account for the unknown attempt frequency ν. The phonon assisted tunneling rate parameters $\alpha_1 = 2.5 \times 10^{-2}$, $\alpha_2 = 0.7 \times 10^{-2}$, confinement length $l_{conf} = 8$ nm, and temperature of the Fermi distribution $T_f = 10$ K are chosen to fit the model to the data. The temperature parameter is chosen higher than the cryostat temperature of 4.2 K to additionally account for broadening of the Fermi energy in the 2DEG due to disorder. We stress that the contributions of elastic tunneling into the 2DEG subbands are calculated with only the quantum dot confinement length l_{conf} and the parameter T_f for broadening of the 2DEG Fermi edge as fitting parameters. A characteristic spatial confinement length for electrons in the QDs of $l_{conf} = 8$ nm agrees with results by Beckel *et al.* on self-assembled QDs grown under similar conditions [10].

In the detuning range of $\Delta E \leqslant 120$ meV, the theoretical calculation reproduces the experimentally observed features well. This supports our assignment to additional tunneling

mechanisms, which in the case of the elastic processes are crucially governed by the lateral wave function overlap of initial QD states and final states in multiple subbands of the 2DEG. Slight deviations are likely caused by the simplicity of the theoretical model: multiple optical phonon modes in GaAs, InAs, and the AlGaAs barrier and ellipticity of the QD shape as well as the impact of the QD size distribution on the wave function are neglected. Significant deviations occur only in the range of $\Delta E > 120$ meV. Here, the calculated position of the third subband energy level deviates from the experimentally observed value as discussed above.

Note that the treatment of phonon-assisted tunneling processes in (1) is not exact, which is why they are included with fitting parameters α_m. We explicitly allow different values of α_1 and α_2, implying different coupling strengths of phonons to final states in the first and second subband. Likely, the observed weaker coupling to states in the second subband around $k_{\mathrm{F,SB2}} = 0$ is related to the higher number of possible phonon momenta that can contribute to tunneling processes if the final states are located at finite k_{F} as is the case in the first subband. Additionally, the overlap integral in z direction changes in the case of the second subband due to the different shape of the quantum well wave function. However, a rigorous calculation of the phonon-assisted tunneling rate is beyond the scope of this paper and is found in Ref. [28].

V. CONCLUSION

We showed that transconductance spectroscopy can be used to study complex elastic and inelastic tunneling dynamics of electrons out of QDs into the subbands of a 2DEG. Notably, the optimal momentum matching between QD s states and free final states at the bottom edge of the second 2DEG subband allows for very efficient tunneling and thus enables all-electrical tuning of the tunneling rate over more than two orders of magnitude. This tuning mechanism differs qualitatively from the previously demonstrated tuning only within the first subband [11], resulting in a larger tuning range: while tuning the tunneling rate via momentum matching within one subband is a continuous process as a function of the applied pulse voltage, additional free states in the second subband become available abruptly. Despite the inhomogeneous broadening caused by the QD ensemble, we were able to identify this fundamental difference from our measurement by comparison to a theoretical model, which is solely based on the lateral wave function overlap between QD and 2DEG states as well as the barrier transmission.

While self-assembled quantum dots in resonant tunneling diode structures have been used before to conduct spectroscopy on the electronic states in a 2DEG, the observations were limited to states in the first, occupied subband and the associated Landau levels in a magnetic field [13,14]. Our study demonstrates that by using transconductance spectroscopy, in which the discharging of electrons from the quantum dots by tunneling into the 2DEG can be studied selectively, also unoccupied higher subbands can be investigated.

Our findings are relevant for novel approaches to all-electrical tunneling spectroscopy and tunnel injection devices in coupled quantum systems. In the case of self-assembled QDs, the shape of the electron wave function in the second 2DEG subband can be used to obtain strongly different tunnel coupling of the 2DEG states to different orbital states in the QDs. As an example, the p-state QD wave function has a node at $k_{x,y} = 0$ and thus exhibits a very small tunnel coupling to states in the 2DEG if the Fermi circle is small as is the case near the subband edges. The maximum tunnel coupling due to optimal momentum matching would then be expected at finite k_{F}. By varying the size of the Fermi circle as demonstrated in our present study, information about the shape of the QD wave function could be obtained from the evolution of the tunneling rate. While wave function imaging of self-assembled QDs has been demonstrated before [15,16], these experiments require an in-plane magnetic field to image the wave function at any point in momentum space other than $k_{x,y} = 0$, which is not required in our method.

Moreover, from an application standpoint, large range all-electrical tuning of the tunneling rate is required for novel QD-based memory devices, featuring long information storage time and fast electronic readout [2,30–32]. Switching between tunneling into the first or second subband of a 2DEG may provide the basis for such a tuning method and can be further optimized by tailoring properties of the semiconductor heterostructure.

The data that support the findings of this study are available from the corresponding author upon reasonable request.

ACKNOWLEDGMENTS

This work was supported by DFG-TRR160, DFG Project No. 383065199, BMBF-Q.Link.X (Grant No. 16KIS0867), and Deutsch-Französische Hochschule (CDFA-05-06).

[1] P. Lodahl, S. Mahmoodian, and S. Stobbe, Rev. Mod. Phys. **87**, 347 (2015).

[2] M. Geller, A. Marent, T. Nowozin, D. Bimberg, N. Akçay, and N. Öncan, Appl. Phys. Lett. **92**, 092108 (2008).

[3] H. Kiyama, A. Korsch, N. Nagai, Y. Kanai, K. Matsumoto, K. Hirakawa, and A. Oiwa, Sci. Rep. **8**, 13188 (2018).

[4] M. Geller, Appl. Phys. Rev. **6**, 031306 (2019).

[5] A. R. Korsch, G. N. Nguyen, M. Schmidt, C. Ebler, S. R. Valentin, P. Lochner, C. Rothfuchs, A. D. Wieck, and A. Ludwig, Phys. Rev. B **99**, 165303 (2019).

[6] D. Najer, I. Söllner, P. Sekatski, V. Dolique, M. C. Löbl, D. Riedel, R. Schott, S. Starosielec, S. R. Valentin, A. D. Wieck *et al.*, Nature (London) **575**, 622 (2019).

[7] L. Zhai, M. C. Löbl, G. N. Nguyen, J. Ritzmann, A. Javadi, C. Spinnler, A. D. Wieck, A. Ludwig, and R. J. Warburton, arXiv:2003.00023v1.

[8] H. Drexler, D. Leonard, W. Hansen, J. P. Kotthaus, and P. M. Petroff, Phys. Rev. Lett. **73**, 2252 (1994).

[9] J. H. Davies, *The Physics of Low-dimensional Semiconductors: An Introduction* (Cambridge University Press, Cambridge, UK, 1998).

[10] A. Beckel, D. Zhou, B. Marquardt, D. Reuter, A. D. Wieck, M. Geller, and A. Lorke, Appl. Phys. Lett. **100**, 232110 (2012).
[11] D. Zhou, A. Beckel, A. Ludwig, A. D. Wieck, M. Geller, and A. Lorke, Appl. Phys. Lett. **106**, 243105 (2015).
[12] A. Thornton, T. Ihn, P. Main, L. Eaves, F. Sheard, and M. Henini, Phys. E (Amsterdam, Neth.) **2**, 657 (1998).
[13] T. Ihn, A. Thornton, I. Itskevich, P. Beton, P. Martin, P. Moriarty, E. Müller, A. Nogaret, P. Main, L. Eaves *et al.*, Phys. Usp. **41**, 122 (1998).
[14] P. C. Main, A. Thornton, R. J. A. Hill, S. T. Stoddart, T. Ihn, L. Eaves, K. A. Benedict, and M. Henini, Phys. Rev. Lett. **84**, 729 (2000).
[15] E. E. Vdovin, A. Levin, A. Patane, L. Eaves, P. C. Main, Y. N. Khanin, Y. V. Dubrovskii, M. Henini, and G. Hill, Science **290**, 122 (2000).
[16] A. Patane, R. J. A. Hill, L. Eaves, P. C. Main, M. Henini, M. L. Zambrano, A. Levin, N. Mori, C. Hamaguchi, Y. V. Dubrovskii, E. E. Vdovin, D. G. Austing, S. Tarucha, and G. Hill, Phys. Rev. B **65**, 165308 (2002).
[17] B. Marquardt, M. Geller, A. Lorke, D. Reuter, and A. D. Wieck, Appl. Phys. Lett. **95**, 022113 (2009).
[18] B. Marquardt, M. Geller, B. Baxevanis, D. Pfannkuche, A. D. Wieck, D. Reuter, and A. Lorke, Nat. Commun. **2**, 209 (2011).
[19] A. Kurzmann, B. Merkel, B. Marquardt, A. Beckel, A. Ludwig, A. D. Wieck, A. Lorke, and M. Geller, Phys. Status Solidi B **254**, 1600625 (2017).
[20] A. Beckel, A. Kurzmann, M. Geller, A. Ludwig, A. D. Wieck, J. König, and A. Lorke, Europhys. Lett. **106**, 47002 (2014).
[21] K. Eltrudis, A. Al-Ashouri, A. Beckel, A. Ludwig, A. Wieck, M. Geller, and A. Lorke, Appl. Phys. Lett. **111**, 092103 (2017).
[22] A. Ludwig, J. H. Prechtel, A. V. Kuhlmann, J. Houel, S. R. Valentin, R. J. Warburton, and A. D. Wieck, J. Cryst. Growth **477**, 193 (2017).
[23] S. Fafard, Z. R. Wasilewski, C. N. Allen, D. Picard, M. Spanner, J. P. McCaffrey, and P. G. Piva, Phys. Rev. B **59**, 15368 (1999).
[24] See Supplemental Material at http://link.aps.org/supplemental/10.1103/PhysRevB.102.035413 for the charging spectrum of the device.
[25] M. C. Löbl, S. Scholz, I. Söllner, J. Ritzmann, T. Denneulin, A. Kovács, B. E. Kardynal, A. D. Wieck, A. Ludwig, and R. J. Warburton, Commun. Phys. **2**, 93 (2019).
[26] S. Birner, T. Zibold, T. Andlauer, T. Kubis, M. Sabathil, A. Trellakis, and P. Vogl, IEEE Trans. Electron Devices **54**, 2137 (2007).
[27] R. J. Warburton, B. T. Miller, C. S. Dürr, C. Bödefeld, K. Karrai, J. P. Kotthaus, G. Medeiros-Ribeiro, P. M. Petroff, and S. Huant, Phys. Rev. B **58**, 16221 (1998).
[28] S.-W. Chang, S.-L. Chuang, and N. Holonyak, Jr., Phys. Rev. B **70**, 125312 (2004).
[29] E. E. Vdovin, Y. N. Khanin, O. Makarovsky, Y. V. Dubrovskii, A. Patanè, L. Eaves, M. Henini, C. J. Mellor, K. A. Benedict, and R. Airey, Phys. Rev. B **75**, 115315 (2007).
[30] A. Marent, T. Nowozin, M. Geller, and D. Bimberg, Semicond. Sci. Technol. **26**, 014026 (2010).
[31] T. Nowozin, A. Beckel, D. Bimberg, A. Lorke, and M. Geller, Appl. Phys. Lett. **104**, 053111 (2014).
[32] L. Bonato, E. M. Sala, G. Stracke, T. Nowozin, A. Strittmatter, M. N. Ajour, K. Daqrouq, and D. Bimberg, Appl. Phys. Lett. **106**, 042102 (2015).